



# UWB/IMU Fusion Localization in Coal Mine Faces Using Improved Particle Filter

Junyan Qi<sup>1</sup>, Yuxue Sun<sup>2,\*</sup>, Lei Wang<sup>2</sup>, Zhuli Ren<sup>3</sup>

<sup>1</sup>School of Software, Henan Polytechnic University, Jiaozuo 454000, Henan, China.

<sup>2</sup>School of Computer Science and Technology, Henan Polytechnic University, Jiaozuo 454000, Henan, China.

<sup>3</sup>School of Energy Science and Engineering, Henan Polytechnic University, Jiaozuo 454000, Henan, China.

**How to cite this paper:** Junyan Qi, Yuxue Sun, Lei Wang, Zhuli Ren. (2026) UWB/IMU Fusion Localization in Coal Mine Faces Using Improved Particle Filter. *Advances in Computer and Communication*, 7(1), 22-37.

DOI: 10.26855/acc.2026.03.004

**Received:** December 31, 2025

**Accepted:** January 29, 2026

**Published:** March 2, 2026

\***Corresponding author:** Yuxue Sun, School of Computer Science and Technology, Henan Polytechnic University, Jiaozuo 454000, Henan, China.

## Abstract

Positioning systems in underground coal mines are challenged by severe multipath propagation and electromagnetic interference, resulting in non-line-of-sight (NLOS) ranging errors and inertial drift. This study proposes a breakthrough cooperative Ultra-Wideband (UWB)-Inertial Measurement Unit (IMU) positioning framework integrating an enhanced Particle Filter (PF) architecture, aimed at delivering a high-precision and robust solution for personnel positioning in high-risk underground coal mining areas. First, a hybrid error compensation model integrating Taylor Series Expansion (TSE) and Sage-Husa Unscented Kalman Filter (SH-UKF) is constructed. The TSE method linearizes NLOS errors in UWB ranging values through polynomial approximation, while SH-UKF dynamically estimates residual error coefficients to achieve nonlinear correction of compensation quantities. Subsequently, a Hunter-Prey Optimization-based Adaptive Weighted Particle Filter (HPO-AWPF) is proposed. This algorithm enhances the global search capability of HPO by introducing adaptive weight factors and designing a Mahalanobis Distance-based adaptive weight allocation strategy to optimize the probability density matching of UWB/IMU observation data. The experimental results demonstrate that the proposed algorithm can alleviate the influence of nonlinear observation on the distribution of particles, effectively solve the problem of particle degradation, and has better robustness and positioning accuracy compared with existing algorithms.

## Keywords

Ultra-Wideband; Inertial Navigation; Hunter Prey Optimization; Adaptive Particle Filter; Multi-Sensor Fusion Localization

## 1. Introduction

The intelligent construction of coal mines is an important initiative to promote the safe development of mines and guarantee the safety of national energy resources [1]. Underground positioning systems constitute a critical component in intelligent coal mine operations, enabling real-time personnel tracking and equipment monitoring to substantially mitigate safety risks in subterranean environments [2]. With the closed space and complex electromagnetic environment of underground coal mines, the positioning and navigation of equipment and personnel have always been a difficult problem [3]. Therefore, the development of high-precision positioning technology for miners and underground equipment is of great significance to enhance the safety of coal mining and promote the innovation of coal mining technology. It can not only effectively reduce the risk of coal mine safety, but also promote the intelligent upgrade of mining operations [4].

Currently, commonly used positioning technologies such as Global Positioning System (GPS), Bluetooth, ultrasonic, etc., can not meet the requirements of positioning accuracy due to the closed space and complex environment of underground coal mines [5, 6]. In contrast, Ultra-Wideband (UWB) positioning technology has become the primary choice for underground positioning in coal mines due to its high-precision positioning, low power consumption, and strong anti-jamming characteristics [7]. UWB positioning technology can provide highly accurate and reliable positioning information under line-of-sight (LOS) conditions [8]. However, in indoor environments with complex layouts and numerous obstacles, UWB devices often operate under non-line-of-sight (NLOS) conditions, which significantly degrade their positioning accuracy [9]. Inertial Measurement Units (IMU) possess advantages of autonomous localization and high-frequency response, but suffer from two fundamental limitations: (1) time-dependent error drift accumulation, and (2) the inability to autonomously determine initial position [10, 11]. The IMU error continues to accumulate, and the UWB error jumps abruptly, both of which cannot individually meet the high-precision localization requirements of complex closed scenes [12]. For this reason, the UWB/IMU tightly coupled system has become the focus of research, through the fusion of the absolute position constraints of UWB and the high-frequency motion data of IMU, combined with intelligent filtering algorithms to realize dynamic compensation of errors, effectively breaking through the performance boundary of a single sensor.

Literature [13] proposes a fusion localization system of UWB and IMU, focusing on solving the localization error problem in non-line-of-sight environments. It is based on an extended Kalman filter (EKF) and UWB's channel impulse response (CIR), and combined with the support vector machine (SVM) for NLOS detection. Literature [14] fully integrates the advantages of UWB's strong resistance to multipath interference and high ranging accuracy, as well as IMU's good short-term stability and high data updating rate by constructing a motion constraint model to correct UWB ranging data in real-time and adopting a fuzzy adaptive Kalman filtering algorithm to realize the fusion of multi-source data. This integrated positioning approach successfully addresses two critical challenges: NLOS propagation errors and inertial navigation drift accumulation. Experimental validation demonstrates sub-meter accuracy in dynamic scenarios, with system stability surpassing conventional fusion schemes. However, the manual calibration of empirical parameters in the motion constraint model introduces scenario dependency, potentially limiting the algorithm's universality across diverse environments. Literature [15] dynamically weighted fusion of data from two types of sensors by an improved extended Kalman filter algorithm not only significantly improves the robustness of localization in complex environments, but also effectively suppresses the cumulative error of inertial navigation. However, this method does not fully consider the dynamic adjustment of fusion weights when the UWB system transitions between LOS/NLOS environments, which may lead to suboptimal error suppression in complex multipath scenarios. Additionally, the single IMU architecture limits its ability to compensate for deterministic errors inherent in inertial measurement units.

Aiming at the localization misalignment problem caused by the significant multipath effect of UWB signals and the accumulation of IMU inertial drift in the underground complex environment, this paper proposes a UWB/IMU cooperative localization algorithm based on improved particle filtering. The proposed method first develops an IMU bias error compensation model using Taylor series expansion (TSE), and then applies the Sage-Husa Unscented Kalman filter (UKF) to dynamically correct UWB ranging residuals; Thereby designing a fusion framework based on Hunter-Prey Optimization and Adaptive Weighted Particle Filter (HPO-AWPF) to achieve probabilistic matching and dynamic weighted fusion of UWB high-precision ranging data and IMU high-frequency motion data. The innovations of this paper are mainly reflected in: 1) Constructing a joint error compensation mechanism integrating TSE linearization compensation and SH-UKF nonlinear mapping correction, which significantly suppresses UWB aberrant ranging and IMU zero-bias drift; 2) a Hunter-Prey Optimization and Adaptive Weighted Particle Filter algorithm is proposed, which dynamically optimizes particle distribution by simulating the local tracking mechanism of hunters and global escape behavior of prey, effectively mitigating particle degeneracy issues.

## 2. Principles of Positioning Technology

### 2.1 UWB Positioning Principles

UWB technology is a new type of wireless communication technology. Unlike traditional communication systems that require carrier waves for data transmission, UWB transmits data by sending and receiving nanosecond or even sub-nanosecond duration pulses. In this method, each information bit can be mapped into hundreds of such pulses [16, 17]. According to the Fourier time-frequency transformation principles, the shorter the time-domain duration of

a single-cycle UWB pulse, the wider the corresponding frequency-domain bandwidth. These nanosecond-scale pulses typically produce a bandwidth on the order of GHz, which gives UWB signals extremely high time resolution and makes them highly suitable for high-precision localization [18].

The basic principle of UWB positioning technology is to measure the distance between two radio transceivers by calculating the time of flight (TOF) of the signal and multiplying it by the speed of light. Common methods include Time Difference of Arrival (TDOA), Two-Way Range (TWR), and Phase Difference of Arrival (PDOA). Among these, the most widely used for positioning is the TDOA method [19].

In underground dynamic localization scenarios, the NLOS propagation error caused by tunnel structure deformation and moving obstacles causes UWB-ranging values to exhibit time-varying nonlinear deviations. For this reason, this paper proposes integrating IMU measurement data to offset the effects of NLOS errors.

## 2.2 IMU Positioning Principle

An IMU is a device that measures the angular velocity and acceleration of an object in three axes. It integrates gyroscopes and accelerometers, providing six degrees of freedom (6-DOF) to measure angular velocity and linear acceleration in three-dimensional space. Adding magnetometers to the accelerometers and gyroscopes creates a "9-axis IMU" [20]. The positioning principle of the IMU can be summarized as follows:

(1) The initial position and initial attitude of the localized target are known, i.e., the position  $(X, Y, Z)$  under the 3D world coordinate system, and the *yaw*, *pitch*, *roll*  $(\alpha, \beta, \gamma)$  under its coordinate system;

(2) Continuously measure the acceleration  $(a_x, a_y, a_z)$  of the localized target in the world coordinate system, and integrate the time quadratically to obtain the trajectory as well as the current position [21]  $(X_c, Y_c, Z_c)$ ;

First integral with respect to time:

$$\begin{aligned} v_x[k] &= v_x[k-1] + \int_{t_{k-1}}^{t_k} a_x(t) dt \approx v_x[k-1] + a_x[k] \cdot \Delta t \\ v_y[k] &= v_y[k-1] + \int_{t_{k-1}}^{t_k} a_y(t) dt \approx v_y[k-1] + a_y[k] \cdot \Delta t \\ v_z[k] &= v_z[k-1] + \int_{t_{k-1}}^{t_k} a_z(t) dt \approx v_z[k-1] + a_z[k] \cdot \Delta t \end{aligned} \quad (1)$$

Where  $v_x[k]$ ,  $v_y[k]$ ,  $v_z[k]$  are the velocity components at time step k,  $a_x[k]$ ,  $a_y[k]$ ,  $a_z[k]$  are the corresponding acceleration components, and  $\Delta t$  is the time step.

Second integral with respect to time:

$$\begin{aligned} X_c[k] &= X_c[k-1] + \int_{t_{k-1}}^{t_k} v_x(t) dt \approx X_c[k-1] + v_x[k] \cdot \Delta t \\ Y_c[k] &= Y_c[k-1] + \int_{t_{k-1}}^{t_k} v_y(t) dt \approx Y_c[k-1] + v_y[k] \cdot \Delta t \\ Z_c[k] &= Z_c[k-1] + \int_{t_{k-1}}^{t_k} v_z(t) dt \approx Z_c[k-1] + v_z[k] \cdot \Delta t \end{aligned} \quad (2)$$

Where  $X_c[k]$ ,  $Y_c[k]$  and  $Z_c[k]$  are the position components at time step k, respectively.

(3) The current attitude can be obtained by continuously measuring the change in attitude angle in the localized target's coordinate system, or by continuously measuring the angular velocity and integrating it over time [22].

$$\begin{aligned} \theta_x[k] &= \theta_x[k-1] + \int_{t_{k-1}}^{t_k} \omega_x(t) dt \approx \theta_x[k-1] + \omega_x[k] \cdot \Delta t \\ \theta_y[k] &= \theta_y[k-1] + \int_{t_{k-1}}^{t_k} \omega_y(t) dt \approx \theta_y[k-1] + \omega_y[k] \cdot \Delta t \\ \theta_z[k] &= \theta_z[k-1] + \int_{t_{k-1}}^{t_k} \omega_z(t) dt \approx \theta_z[k-1] + \omega_z[k] \cdot \Delta t \end{aligned} \quad (3)$$

Where  $\theta_x[k]$ ,  $\theta_y[k]$  and  $\theta_z[k]$  are the angular change in attitude around the x, y, and z axes at time step k, respectively, and  $\omega_x[k]$ ,  $\omega_y[k]$ ,  $\omega_z[k]$  are the corresponding angular velocity components.

### 2.3 Principles of the PF Algorithm

The basic idea of the particle filtering (PF) algorithm is to select an important probability density and randomly sample from it, get some random samples with corresponding weights, adjust the size of the weights and the position of the particles based on the state observation, and then use these samples to approximate the state a posteriori distribution, and then finally use the weighted summation of this set of samples as the estimation value of the state [23].

The following are the main steps of the particle filtering algorithm [24]:

(1) At the initial moment,  $N$  samples  $\{x_0^n\}_{n=1}^N$  are drawn from the a priori probability density function  $p(x_0)$ , and each sample is assigned the same weight  $\omega_0^n = \frac{1}{N}$ .

(2) At each discrete time instant  $k$ , a set of samples is drawn from the importance density function  $q(x_k|x_{0:k-1}, z_{1:k})$ . Often,  $q$  is chosen to be the prior probability density  $p(x_k|x_{k-1})$  or some other easily sampled distribution to simplify the computation.

(3) The weights of the particles are updated based on the observed data  $Z_k$ . The formula for weight update is:

$$\omega_k^n \propto \omega_{k-1}^n \cdot p(z_k | x_k^n) \quad (4)$$

Where  $\omega_k^n$  is the weight of the  $n$ th particle at moment  $k$ , and  $p(z_k|x_k^n)$  is the observation model that represents the probability of observing  $z_k$  in state  $x_k^n$ . The weights are also normalized after they are updated.

(4) To avoid the particle degradation problem, resampling is also performed based on the weights of the particles. During the resampling process, particles with larger weights will be selected multiple times, while particles with smaller weights may be eliminated.

(5) Use the updated set of particles to approximate the posterior probability density and compute the state estimate. The state estimate can be calculated using the following equation:

$$\hat{x}_k = \sum_{n=1}^N \omega_k^n x_k^n \quad (5)$$

Where  $\hat{x}_k$  is the state estimation based on the particle set  $\{x_k^n\}_{n=1}^N$  and weights  $\{\omega_k^n\}_{n=1}^N$ .

(6) Pass the set of particles to the next moment, i.e.,  $x_{k+1}^n \sim p(x_{k+1}|x_k^n)$ .

### 3. Combined Positioning System

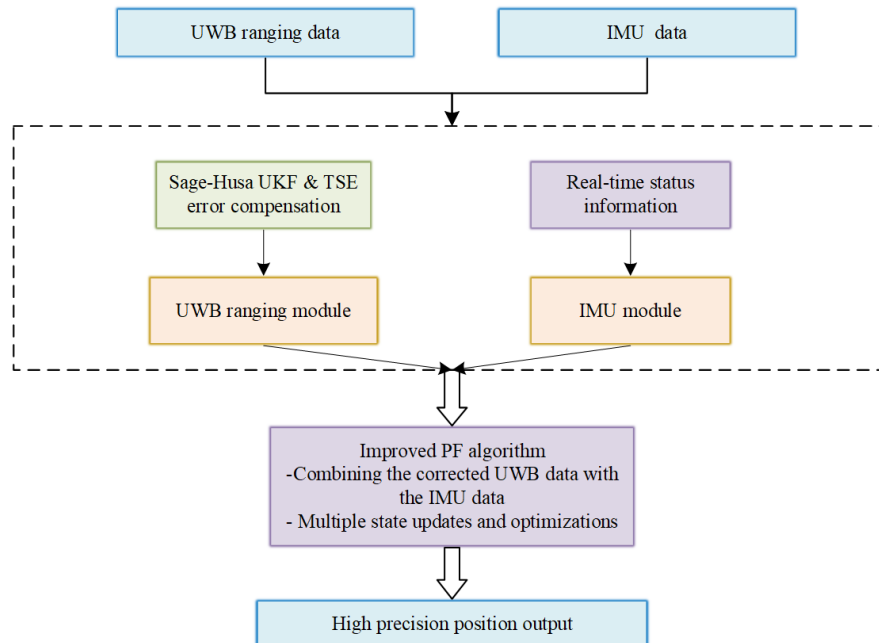


Figure 1. Schematic Diagram of the UWB /IMU Integrated Positioning System.

As shown in Figure 1, the UWB ranging module is first utilized to obtain the direct measurement distance between the tag and the base station, and due to the large NLOS in the coal mine underground, the UWB measurement data are preprocessed using the Taylor Series Expansion (TSE) method to compensate for the systematic and nonlinear errors; and then the Unscented Kalman Filter (UKF) is applied to the TSE-preprocessed data for further filtering and state estimation. At the same time, the IMU module continuously collects the acceleration and angular velocity data of the tag, which is processed by the inertial navigation algorithm to derive the real-time state information of the tag. Next, the ranging data corrected by Sage-Husa UKF and TSE are used as inputs to the improved particle filtering algorithm. The improved PF algorithm combines the position information provided by the inertial navigation algorithm to construct the ranging equations for state estimation, which in turn performs the state update step. This process is optimized with several filtering optimizations and finally achieves highly accurate positioning of people in the coal mine working face.

### 3.1 Sage-Husa UKF-TSE Ranging Error Correction

UWB signals have the advantages of large frequency domain bandwidth and high time resolution, which can maintain good signal stability and anti-interference ability in the harsh environment of underground coal mines, and therefore have a wide range of application prospects in underground coal mine positioning systems. However, its ranging error is an important factor affecting positioning accuracy. The Sage-Husa Kalman Filter (SHKF) algorithm is a filtering algorithm used for state estimation, which has the advantages of high flexibility in application and high accuracy in estimation results [25], but it is sensitive to the initial value of the noise parameter in the nonlinear scenario, and poorly adapted to the non-Gaussian error. UKF accurately conveys the statistical properties of nonlinear systems through the untraced transform and achieves high-order moment estimation with  $O(n)$  computational complexity while avoiding the linearization error of the Jacobi matrix, which significantly improves the state estimation accuracy and numerical stability in non-Gaussian noise scenarios [26]. To improve the accuracy of UWB ranging, this paper extends the SHKF to the Sage-Husa untraceable Kalman filter (SH-UKF), which realizes the accurate transmission of the statistical properties of the nonlinear system through the untraceable transformation; at the same time, the first-order linearization preprocessing is performed on the UWB ranging equations by using the TSE to suppress the nonlinear propagation of NLOS and to realize the correction of UWB ranging errors.

It is known that the coordinates of  $n$  reference base stations are  $(x_1, y_1), (x_2, y_2), \dots, (x_n, y_n)$ . The distance residual function  $f_i(x, y)$  is defined to characterize the discrepancy between the geometric distance from the tag coordinates  $(x, y)$  to the  $i$ -th base station and the UWB ranging measurement  $r_i$ . When  $f_i(x, y)$  approaches zero, it indicates that the estimated coordinates  $(x, y)$  achieve optimal alignment with the ranging results from the  $i$ -th base station. By constructing a system of residual equations across  $n$  base stations, a nonlinear least squares optimization model can be established as follows:

$$f_i(x, y) = \sqrt{(x - x_i)^2 + (y - y_i)^2} - r_i \quad (6)$$

For the UWB nonlinear ranging equations, the Taylor series expansion of the distance equation from each base station to the tag at  $x_0$  is performed, retaining the first-order terms and ignoring the higher-order minima to approximate the nonlinear function as a linear equation:

$$f_i(x, y) \approx f_i(x_0, y_0) + \frac{\partial f_i}{\partial x}(x_0, y_0)(x - x_0) + \frac{\partial f_i}{\partial y}(x_0, y_0)(y - y_0) \quad (7)$$

Where  $\frac{\partial f_i}{\partial x}(x_0, y_0)$  and  $\frac{\partial f_i}{\partial y}(x_0, y_0)$  are the partial derivatives of  $f_i$  at  $(x_0, y_0)$  with respect to  $x$  and  $y$ , respectively:

$$\begin{aligned} \frac{\partial f_i}{\partial x}(x_0, y_0) &= \frac{x_0 - x_i}{\sqrt{(x_0 - x_i)^2 + (y_0 - y_i)^2}} = J_{i,x} \\ \frac{\partial f_i}{\partial y}(x_0, y_0) &= \frac{y_0 - y_i}{\sqrt{(x_0 - x_i)^2 + (y_0 - y_i)^2}} = J_{i,y} \end{aligned} \quad (8)$$

The linearized equations for all the base stations are combined to construct the Jacobian matrix  $J$  and residual vector  $v$ :

$$J = \begin{bmatrix} \frac{\partial f_1}{\partial x} & \frac{\partial f_1}{\partial y} \\ \frac{\partial f_2}{\partial x} & \frac{\partial f_2}{\partial y} \\ \vdots & \vdots \\ \frac{\partial f_N}{\partial x} & \frac{\partial f_N}{\partial y} \end{bmatrix} \quad (9)$$

$$v = \begin{bmatrix} f_1(x_0, y_0) \\ f_2(x_0, y_0) \\ \vdots \\ f_N(x_0, y_0) \end{bmatrix}$$

The correction  $\Delta X$  is found by solving the following linear least squares problem:

$$J\Delta X = -v \quad (10)$$

Update the position estimate using  $\Delta X$ :

$$X_1 = X_0 + \Delta X \quad (11)$$

Use  $X_1$  as the new initial estimate, and repeat the above steps until the iteration termination conditions are satisfied: (1) the correction  $\Delta X$  is small enough; (2) the preset number of iterations is reached. When the iteration terminates, the final estimate is the optimal solution  $(x_D, y_D)$  close to the true coordinates.

The UWB localization results initially reduce the NLOS error by the TSE error compensation method, but its measurements still have some errors with the real distance, so the SH-UKF is used for further optimization. The Sage-Husa noise estimator is introduced based on the traditional UKF, and the sigma point sampling of the nonlinear system state is performed by the untraceable transform (UT) to avoid the Jacobi matrix computation; meanwhile, the real-time estimation of the system noise covariance matrix  $Q_k$  and the observation noise covariance  $R_k$  is performed to dynamically compensate for the effect of the sudden change of the downhole environmental noise. The TSE-optimized measurement results are input into the SH-UKF as observations for further filtering operations, taking advantage of its noise adaptive capability and nonlinear processing, to achieve high-precision position prediction in dynamic environments. The flowchart of the Sage-Husa UKF-TSE ranging error correction is shown in Figure 2.

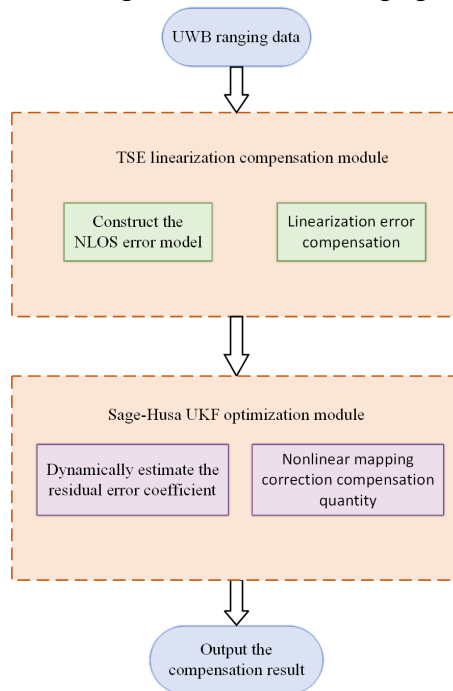


**Figure 2. A Collaborative Correction Framework for UWB Ranging Errors Based on TSE Linearization and SH-UKF Optimization.**

### 3.2 Hunter Prey Optimization and Adaptive Weighted Fusion-based Particle Filtering

The traditional particle filtering algorithm has the following limitations:

(1) Particle degradation: after several iterations, the weights of most particles will be concentrated on a few particles, leading to a reduction in sample diversity.

(2) High computational complexity: a large number of particles are needed to ensure the filtering performance, especially in high-dimensional states.

To address the above limitations, the following improvement strategies are proposed in this paper. Aiming at the problems of NLOS interference of UWB signals in the coal mine working face and the cumulative error of IMU, an improved particle filtering algorithm (HPO-AWPF) integrating hunter-prey optimization (HPO) and adaptive weighted fusion of UWB/IMU is proposed. The HPO algorithm is a meta-heuristic algorithm inspired by predatory behavior in nature, and its core idea simulates the following ecological dynamics processes [27]. (1) Hunter role: represents the better-adapted individuals (elite particles) in the search space, and realizes local fine search by actively tracking the prey (optimal solution direction). (2) Prey role: represents individuals with lower adaptability (ordinary particles), exploring the unknown region through random escape behaviors (e.g., Levi's flight) to avoid falling into the local optimum. (3) Dynamic interaction: there is a game between the hunter and the prey to update their positions, and the pursuit strategy of the hunter and the escape strategy of the prey drive the population to converge to the global optimal region.

The algorithm framework is shown in Figure 3, which contains the following core modules: (1) HPO particle optimization: optimize the particle distribution before resampling to improve the convergence efficiency; (2) adaptive weighted fusion: dynamically assign UWB/IMU weights to suppress sensor noise interference; (3) residual resampling: retain the high-weight particles to maintain the diversity of samples.

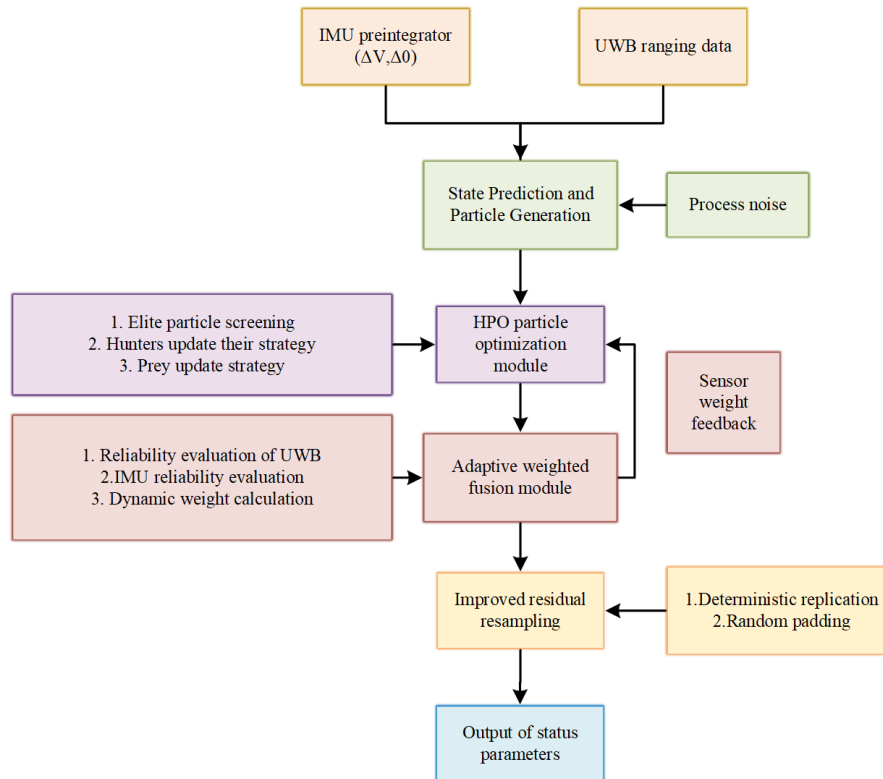


Figure 3. Framework of the HPO-AWPF Algorithm.

#### 1) State prediction and particle propagation

Predict the next moment position of particles from IMU data as the initial distribution for HPO optimization. Input the last-moment particle set  $\{x_{k-1}^{(i)}, \omega_{k-1}^{(i)}\}_{i=1}^N$ , IMU pre-integrated quantities  $\Delta v_k$  (velocity increment) and  $\Delta \theta_k$  (angle increment). The state propagation model is:

$$\mathbf{x}_k^{(i)} = f(\mathbf{x}_{k-1}^{(i)}) + \mathbf{B} \cdot \begin{bmatrix} \Delta \mathbf{v}_k \\ \Delta \theta_k \end{bmatrix} + \mathbf{w}_k^{(i)} \quad (12)$$

Where  $\omega_k^{(i)} \sim N(0, Q_k)$ ,  $f(x)$  is the nonlinear state transfer function (e.g., kinematic model),  $B$  represents the mapping matrix of IMU measurements to state quantities, and  $Q_k$  is the process noise covariance matrix characterizing the IMU error characteristics.

2) Layered optimization-convergence mechanism

(1) Inner layer: HPO particle optimization

Step1: Elite Particle Screening

The top 30% are selected as hunters (elite particles) based on the product of the particle weights  $\omega^{(i)}$  and the observation likelihood  $p(z_k | \mathbf{x}^{(i)})$ :

$$S_H = \mathbf{x}^{(i)} | w^{(i)} \cdot p(z_k | \mathbf{x}^{(i)}) \geq \eta \cdot \max(w^{(j)} \cdot p(z_k | \mathbf{x}^{(j)})), \quad \eta = 0.7 \quad (13)$$

Where  $\eta$  represents the elite threshold to dynamically screen high-likelihood particles.

Step2: Hunter-prey differentiation update

Hunter update (local development)

Hunter particles rely on IMU weights to enhance localized tracking for continuous motion scenarios.

$$\mathbf{x}_{\text{new}}^{(i)} = \mathbf{x}^{(i)} + \alpha \cdot (\mathbf{x}^* - \mathbf{x}^{(i)}) + \beta \cdot \frac{w_{\text{IMU}}}{w_{\text{IMU}} + w_{\text{UWB}}} \cdot \mathbf{r}_1 \odot (\mathbf{x}^* - \mathbf{x}^{(i)}) \quad (14)$$

Where  $\alpha = 0.5 + 0.3 \tanh(5\omega_{\text{IMU}})$ , increases the local search intensity when the IMU weight is high.  $\beta = 0.2$  is a perturbation factor to prevent from falling into a local optimum.  $\mathbf{r}_1 \in [0,1]^d$  denotes a uniformly distributed random vector.

Prey update (global exploration)

Prey particles utilize UWB weights to drive wide-area search and suppress NLOS errors.

$$\mathbf{x}_{\text{new}}^{(j)} = \mathbf{x}^{(j)} + \gamma \cdot \text{Levy}(\lambda) \odot (w_{\text{UWB}} \cdot (\mathbf{z}_{\text{UWB}} - h(\mathbf{x}^{(j)})) + w_{\text{IMU}} \cdot (\mathbf{z}_{\text{IMU}} - h(\mathbf{x}^{(j)}))) \quad (15)$$

Where  $\gamma = 1.2 + 0.6\omega_{\text{UWB}}$ , which extends the search range when the UWB weights are high;  $\text{Levy}(\lambda)$  denotes the Levy flight randomization step, which generates long jump paths with heavy-tailed distributions; and  $h(x)$  is the observation modeling function, which maps the state to the sensor measurement space.

(2) Outer layer: adaptive weighted fusion

Step 1: sensor reliability assessment

UWB reliability factor:

$$\rho_{\text{UWB}} = \exp\left(-\frac{\sigma_{\text{UWB}}^2}{R_t}\right), \quad R_t = \frac{1}{N} \sum_{i=1}^N \|\mathbf{z}_{\text{UWB}} - h(\mathbf{x}^{(i)})\|^2 \quad (16)$$

$\sigma_{\text{UWB}}^2$  denotes the preset UWB measurement noise variance.  $\mathbf{r}_t$  denotes the observation residual at the current moment, reflecting the degree of UWB anomalies. NLOS determination condition: if  $\rho_{\text{UWB}} < 0.3$ , it is determined as NLOS state, which triggers the prey particle Lévy search.

IMU Reliability Factor:

$$\rho_{\text{IMU}} = \frac{1}{1 + \|\nabla \mathbf{a}_k\|_2}, \quad \nabla \mathbf{a}_k = \mathbf{a}_k - \mathbf{a}_{k-1} \quad (17)$$

$\nabla \mathbf{a}_k$  denotes the acceleration differential, which serves to detect violent motion or vibration disturbances.

Step 2: Dynamic weighting

$$w_{\text{UWB}} = \frac{\rho_{\text{UWB}}}{\rho_{\text{UWB}} + \rho_{\text{IMU}}}, \quad w_{\text{IMU}} = 1 - w_{\text{UWB}} \quad (18)$$

To ensure that the weights are normalized, it is necessary to ensure that  $\omega_{UWB} + \omega_{IMU} = 1$ .

Step 3: Weight Feedback to HPO Parameters

Dynamic regulation of hunter step length  $\alpha$  and prey step length  $\gamma$ :

$$\alpha = 0.5 + 0.3 \cdot \tanh(5w_{IMU}), \quad \gamma = 1.2 + 0.6w_{UWB} \quad (19)$$

When IMU reliability is high ( $\omega_{IMU} \uparrow$ ), increase  $\alpha$  to enhance inertial tracking.

When UWB reliability is high ( $\omega_{UWB} \uparrow$ ), increase  $\gamma$  to extend the search range.

### 3) Improved Residual Resampling

To maintain diversity while retaining highly weighted particles, the algorithm also introduces a residual resampling mechanism. First, replicate  $\lfloor N \cdot \omega^{(i)} \rfloor$  times for each particle, retaining  $N_{copy} = \sum \lfloor N \cdot \omega^{(i)} \rfloor$  particles; and then randomly fill in the residuals, with the remaining  $N_r = N - N_{copy}$  copy particles being sampled with the following probability:

$$P(\mathbf{x}^{(i)}) \propto \exp\left(-\frac{\|\mathbf{x}^{(i)} - \mathbf{x}^*\|^2}{2\sigma_x^2}\right) \cdot (1 - w^{(i)}) \quad (20)$$

Where  $\mathbf{x}^*$  denotes the current optimal estimation state, and  $\sigma_x$  denotes the distance penalty coefficient. By introducing the residual resampling mechanism, low-weight particles still have a chance to be retained if they are far away from the optimal region, avoiding the loss of diversity.

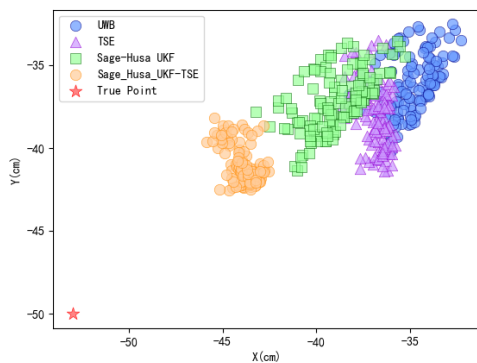
## 4. Experimental Validation and Result Analysis

### 4.1 UWB Non-line-of-sight Error Handling

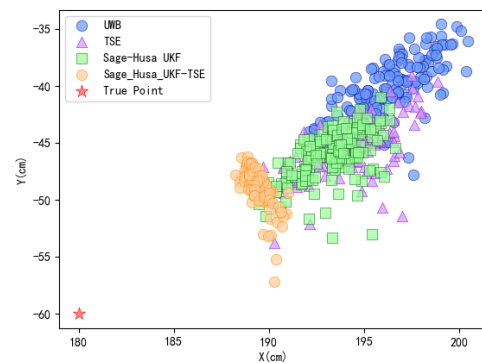
To verify the effectiveness of the Sage-Husa UKF-TSE joint error processing method, this paper will conduct a UWB positioning test experiment. This experiment adopts the medium-range localization module LD150 from Dalian Hao Ru Technology, which uses the STM32F103CBT6 microcontroller as the main control MCU and DW1000 as the core UWB chip. Different obstacles were deployed in the experimental site to simulate the NLOS environment of coal mine tunnels. The UWB anchor nodes were securely fixed at predetermined positions within the experimental site. The UWB mobile nodes were positioned at varying locations to collect ranging data. At each position, 130 repeated measurements were conducted to ensure statistically robust data sampling. The following methods are used to process the data for each set of collected data, respectively:

- Direct use of raw UWB ranging data;
- Application of Sage-Husa UKF to filter the UWB ranging data;
- Application of TSE for error compensation of UWB ranging data;
- Combining the error compensation methods of TSE and Sage-Husa UKF to process the UWB ranging data.

Statistical analysis was performed on the processed ranging results of each group to evaluate the effectiveness of different methods in improving localization accuracy, and conclusions were drawn.



(a)



(b)

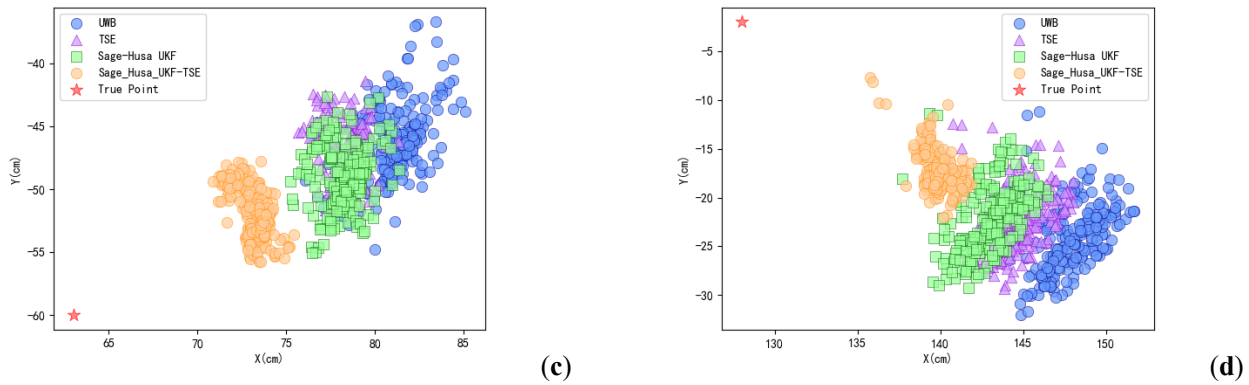


**Figure 4. Effectiveness Evaluation of UWB Ranging Error Processing: (a) Coordinate Point (-53, -50); (b) Coordinate Point (180, -60); (c) Coordinate Point (63, -60); (d) Coordinate Point (128, -2).**

Figure 4 demonstrates the localization results after applying Sage-Husa UKF, TSE, and the joint error processing method of Sage-Husa UKF and TSE at the points with coordinates of (-53, -50), (180, -60), (63, -60), and (128, -2), respectively. The blue dots are the UWB localization data directly measured by Hao Ru Technology LD150, the green squares and purple triangles represent the UWB data processed by the Sage-Husa UKF algorithm and the Taylor series expansion method, respectively, and the yellow dots represent the coordinates solved by applying the joint Sage-Husa UKF and TSE processing method proposed in this paper, and the red pentagrams represent the real coordinates. From the figure, it can be seen that the coordinates represented by the yellow dots are not only closer to the real points marked by the red pentagrams, but also more concentrated in distribution, indicating that the localization results of the joint error processing method of Sage-Husa UKF and TSE are better than those of other methods in terms of accuracy and stability.

Root-mean-square error (RMSE) analysis of the localization results of the four localization methods on the x-axis and y-axis, respectively.

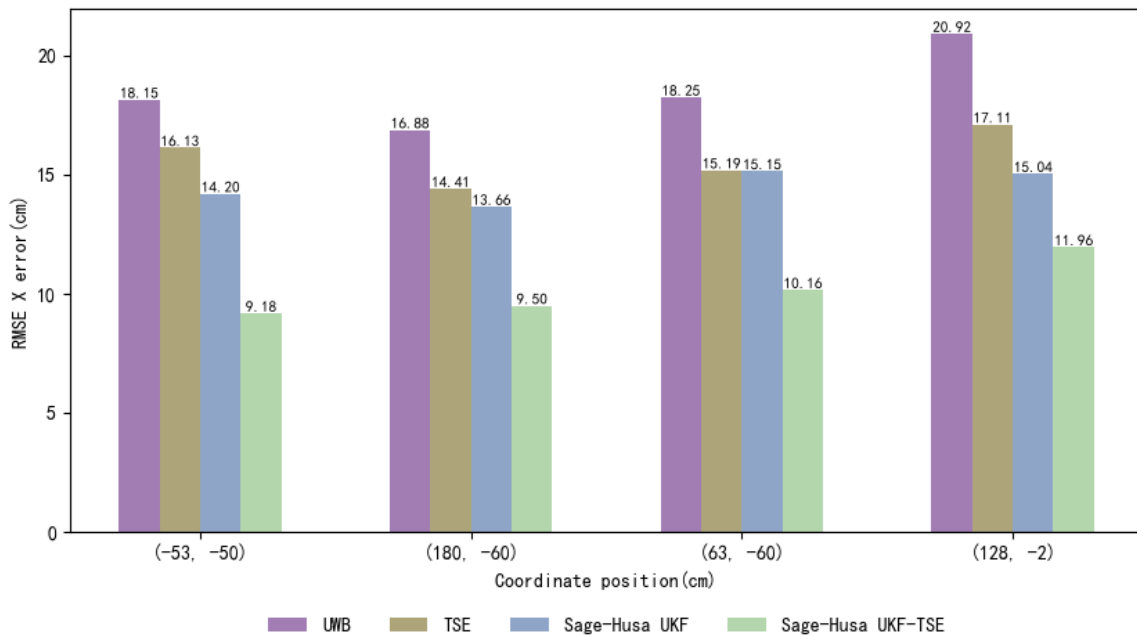


**Figure 5. X-axis RMSE.**

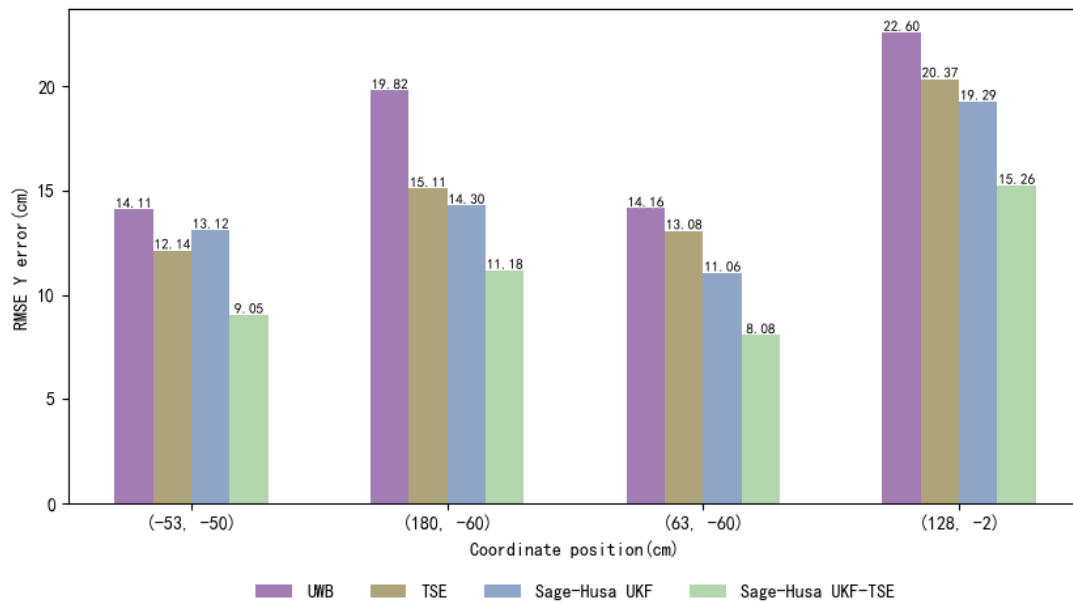


Figure 6. Y-axis RMSE.

The average root mean square error results are shown in Table 1.

From Table 1, it can be seen that the method based on the joint processing of UWB ranging errors by Sage-Husa UKF and TSE achieves good results in the four points taken in the experiment. The TSE algorithm yielded an average RMSE of 15.71 cm along the X-axis and 15.18 cm on the Y-axis, while the Sage-Husa UKF method produced RMSE values of 14.51 cm (X-axis) and 14.44 cm (Y-axis). Notably, the integrated Sage-Husa UKF-TSE method significantly reduced positioning errors to 10.20 cm (X-axis) and 10.89 cm (Y-axis). Compared to standalone TSE, this represents improvements of 35.1% in X-axis accuracy and 28.3% in Y-axis accuracy. When benchmarked against the Sage-Husa UKF alone, accuracy enhancements reached 29.7% (X-axis) and 24.6% (Y-axis). These results conclusively demonstrate the combined algorithm's exceptional capability in suppressing UWB ranging errors, providing robust technical support for high-precision positioning systems.

Table 1. Localization Statistical Results

Processing method	X (cm)	Y (cm)
UWB	18.85	17.67
TSE	15.71	15.18
Sage-Husa UKF	14.51	14.44
Sage-Husa UKF-TSE	10.20	10.89

#### 4.2 Combined UWB/IMU Localization Experiment Based on Improved Particle Filtering

To verify the combined UWB/IMU localization accuracy based on improved particle filtering, an experimental scheme is designed in this paper. The experimental environment simulates the restricted space characteristics of a real mine, adopting a rectangular closed field with a length of 4.5 m×width of 2.8 m, and installing adjustable metal obstacles and dynamic interference sources in the interior to reproduce the complex electromagnetic environment, such as multipath reflections and NLOS bursts in the underground mine. Four UWB base stations are placed at the four corners of the site, and 12 NOKOV motion capture lenses are installed around the site, which can accurately capture the real-time position of the object under test, and the positioning accuracy can reach up to the sub-millimeter level.

The data captured by the NOKOV motion capture system was used as the real trajectory in this experiment.

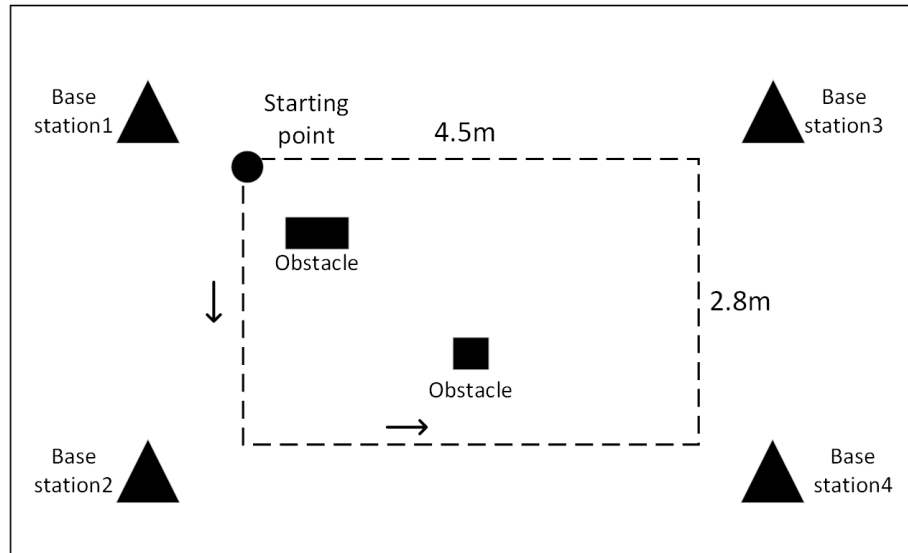


Figure 7. Motion Trajectory.

The Decawave DW1000-based UWB mobile node (integrated with the IMU module) was mounted on the subject's wrist. Sixteen reflective markers were attached to limb joints to capture ground-truth trajectories via a motion capture system. After the experiment commenced, the subject walked around the field for one week. The traditional Particle Filter (PF) algorithm and the proposed improved PF algorithm (HPO-AWPF) were employed to fuse UWB and IMU data, with the number of particles set to 400. To contextualize the fusion performance, positioning trajectories from standalone UWB and IMU systems were also recorded alongside the PF and HPO-AWPF results. The two groups of trajectory plots were comparatively analyzed to draw conclusions.

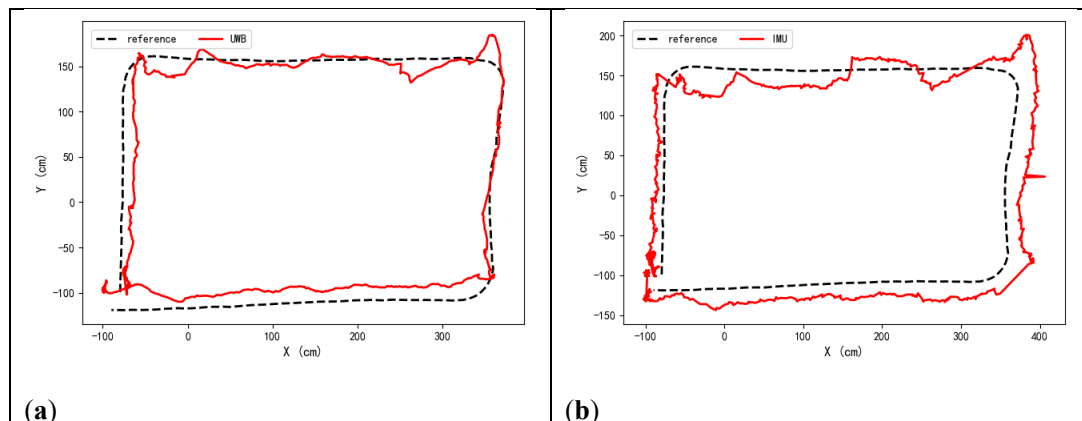
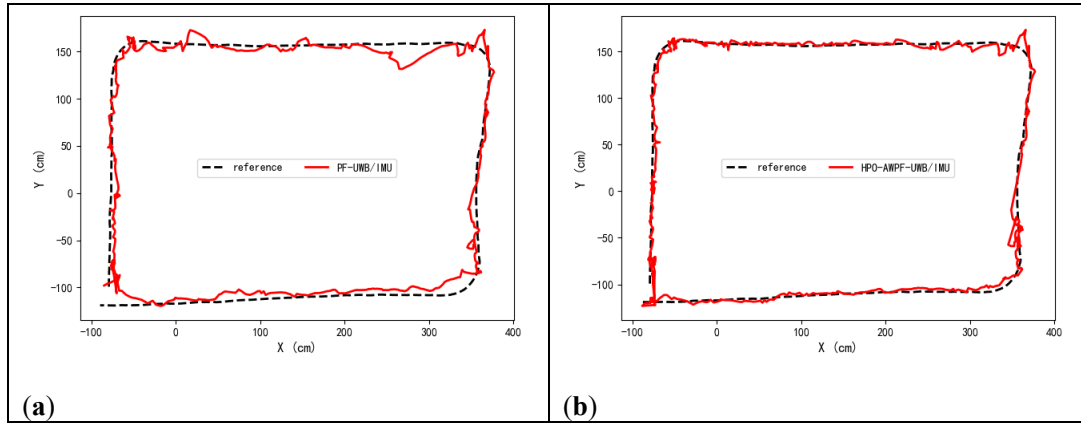


Figure 8. Single sensor positioning track diagram: (a) UWB-only Positioning; (b) IMU-only Positioning.

Experiments conducted using UWB positioning alone are shown in Figure 8(a). The results demonstrate that under standalone UWB localization, the maximum X-axis error is 18.36 cm with a root mean square error (RMSE) of 13.67 cm, while the maximum Y-axis error reaches 18.01 cm with an RMSE of 12.62 cm. Notably, in trajectory-turning areas, UWB signals are susceptible to reflections from surrounding obstacles (e.g., walls and metallic structures). The combined effects of NLOS propagation and multipath interference lead to deviations in Time of Arrival (TOA) estimation, significantly degrading positioning accuracy. Positioning experiments using solely an IMU sensor were conducted, with the results shown in Figure 8(b). The data reveals that under IMU-only localization, the maximum X-axis error reaches 25.73 cm with an RMSE of 16.5 cm, while the maximum Y-axis error is 21.59 cm with an RMSE of 14.86 cm. It can be observed that standalone IMU-based positioning exhibits significant cumulative drift errors, which substantially degrade the system's localization accuracy over time. These findings demonstrate that the positioning accuracy of standalone sensor systems fails to meet high-precision localization requirements.



**Figure 9. Trajectory of UWB-IMU Sensor Fusion Localization: (a) Conventional PF; (b) Enhanced PF (Proposed).**

Figures 9 (a) and (b) illustrate the positioning performance of the UWB/IMU integrated system using conventional particle filtering (PF) and the proposed improved PF algorithm, respectively. The trajectory comparison reveals that the enhanced algorithm developed in this work achieves significantly closer alignment with the ground truth path compared to traditional PF methods, particularly in complex maneuvering segments.

Table 2 presents the error metrics of sensor-only localization versus traditional PF algorithm-based fusion localization. From the comparison of the experimental results, it can be seen that compared with single UWB localization, this paper's algorithm reduces the root mean square error (RMSE) in the X/Y axis by 33.6% and 36.5%, respectively, and improves the comprehensive positioning accuracy by 34.9%; compared with IMU localization, the RMSE of the X/Y axis decreases by 44.9% and 46.0%, and improves the comprehensive accuracy by 45.5%; compared with the traditional PF algorithm, this paper's method reduces the maximum error is reduced by 3.92 cm and 3.08 cm, respectively, and the integrated RMSE is optimized from 15.52 cm to 12.11 cm, with an accuracy improvement of 22.0%. The experiment proves that through the UWB/IMU heterogeneous data fusion and adaptive particle optimization, the algorithm in this paper effectively suppresses the NLOS sudden error, and provides a high-precision and strong robust positioning solution for the complex downhole environment.

**Table 2. Error Statistics of Experimental Results**

	Error/cm	UWB	IMU	PF	HPO-AWPF
X	Maximum value	18.36	25.73	14.56	10.64
	Root mean square	13.67	16.5	12.27	9.08
Y	Maximum value	18.01	21.59	12.93	9.85
	Root mean square	12.62	14.86	9.51	8.02

### 4.3 Multi-Algorithm Localization Performance Benchmarking

To verify the localization performance of the HPO-AWPF algorithm under multi-algorithm fusion in confined mine spaces, traditional PF, bat algorithm-optimized PF (BA-PF), and grey wolf optimizer-optimized PF (GWO-PF) were selected as benchmark comparisons. Horizontal comparative tests were conducted in a simulated underground enclosed experimental field. The number of particles,  $N$ , was set to 400, and the average RMSE and computational time from 10 repeated calculations were used for analysis.

Figure 10 illustrates the dynamic error distributions of four fusion algorithms along the X/Y axes. The PF exhibits a wide fluctuation range of 10.00-16.25 cm on the X-axis and 9.02-13.93 cm on the Y-axis, with its error peaks strongly correlated to metal obstacle-dense regions. In contrast, the HPO-AWPF algorithm compresses the X/Y-axis error ranges to 7.03-10.68 cm and 8.50-10.47 cm, respectively, through dynamic search radius adjustment via Hunter-Prey Optimization (HPO), while reducing standard deviations to  $\pm 1.12$  cm (X-axis) and  $\pm 0.95$  cm (Y-axis). Notably, during electromagnetic interference intervals, HPO-AWPF achieves an X-axis error reduction of 3.08 cm compared to PF, validating its Mahalanobis distance-driven weight allocation strategy in resolving multi-source observation

conflicts. Although the GWO-PF outperforms BA-PF in average error, its computational latency is 15.3% higher than HPO-AWPF, demonstrating the proposed algorithm's superior trade-off between precision and real-time performance in NLOS-dominant environments.

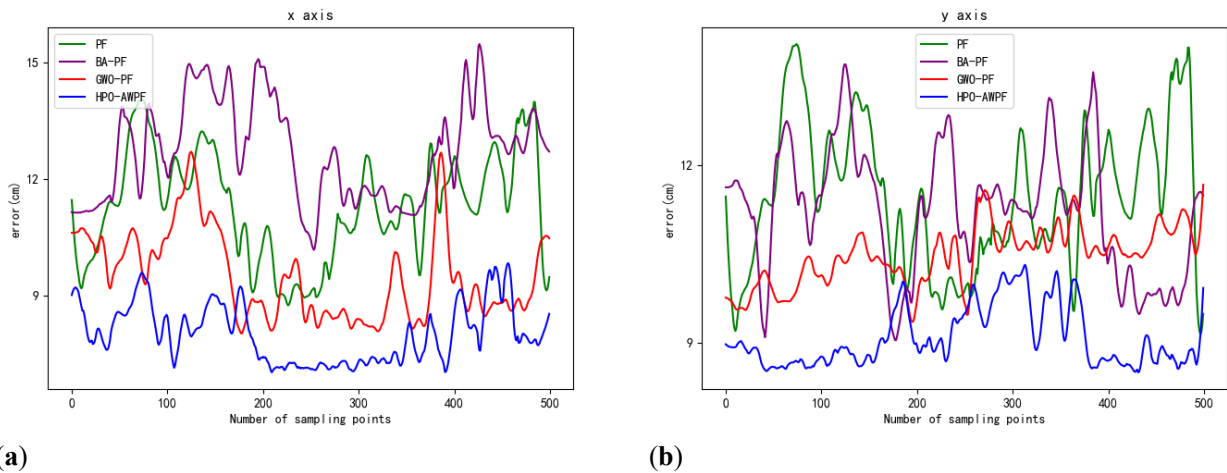


**Figure 10. Error of Partial Sampling Points:(a) Partial Sampling Point Errors on the X-axis; (b) Partial Sampling Point Errors on the Y-axis.**

Table 3 presents the localization error metrics of the four algorithms. As evidenced by the data, the BA-PF, GWO-PF, and HPO-AWPF algorithms demonstrate superior localization accuracy overall compared to the baseline PF method. However, the computational complexity introduced by intelligent optimization algorithms leads to increased runtime. Furthermore, in areas with dense metallic obstacles and during periods of dynamic electromagnetic interference, the traditional PF suffers from significant localization drift caused by nonlinear observations and IMU error accumulation. In contrast, the HPO-AWPF algorithm dynamically adjusts the search range of particle swarms through a hunter-prey optimization mechanism and prioritizes particles with higher consistency to the UWB/IMU joint observation model using Mahalanobis distance-based weight allocation. This approach significantly suppresses state estimation deviations under complex working conditions. Additionally, the adaptive weight factor in the improved algorithm autonomously reinforces IMU angular velocity constraints during electromagnetic interference, effectively balancing the impact of sensor reliability fluctuations on fusion results. Compared to the benchmark algorithms, the HPO-AWPF demonstrates superior spatial consistency. Consequently, in environments with dense metallic obstacles and dynamic electromagnetic interference, the HPO-AWPF exhibits smaller fluctuations in localization error, higher alignment with the true trajectory, and stronger robustness in dynamic NLOS scenarios compared to BA-PF and GWO-PF algorithms.

**Table 3. Positioning accuracy and computation time of different algorithms**

Algorithm	Average RMSE (cm)	Maximum Error (cm)	Average Computation Time (s)
PF	12.14	16.25	0.924
BA-PF	11.27	15.82	1.024
GWO-PF	9.51	12.93	1.309
HPO-AWPF	8.03	10.68	1.206

## 5. Conclusion

Aiming at the difficulties such as significant NLOS errors of UWB signals and dispersion of IMU inertial measurement unit cumulative errors in the complex environment of underground coal mine working faces, this paper proposes a tightly coupled UWB/IMU localization algorithm based on an improved Hunter-Prey Optimized Adaptive Weighted Particle Filter (HPO-AWPF). The method effectively suppresses NLOS errors through a joint error compensation mechanism integrating TSE and Sage-Husa Unscented Kalman Filter (SH-UKF), which enables linearized iterative

correction of nonlinear ranging equations and dynamic noise covariance estimation at the UWB side. Simultaneously, it compensates for UWB localization outliers using IMU short-term high-precision position measurements. Furthermore, the hunter-prey optimization (HPO) algorithm dynamically optimizes particle distribution density and weight updating strategies, solving the positioning drift caused by particle degradation and sensor reliability fluctuations in traditional particle filtering under multipath interference in underground alleyways. Experimental results show that, compared with standalone UWB and IMU localization, the proposed algorithm reduces localization errors by 34.9% and 45.5% in strong NLOS scenarios, with trajectory tracking root mean square error stabilized within 12.1 cm, demonstrating its high accuracy and robustness in dynamic and complex environments.

## References

- [1] Wu X, Li H, Wang B, et al. Review on improvements to the safety level of coal mines by applying intelligent coal mining. *Sustainability*. 2022;14(24):16400.
- [2] Wang H, Chen Y, Wang H. Research and practice on key technologies for intelligentization of coal mine. *Coal Geol Explor*. 2023;51(1):44-54.
- [3] Wang G. New technological progress of coal mine intelligence and its problems. *Coal Sci Technol*. 2022;50(1):1-27.
- [4] Cui Y, Liu S, Liu Q. Navigation and positioning technology in underground coal mines and tunnels: A review. *J South Afr Inst Min Metall*. 2021;121(6):295-303.
- [5] Seguel F, Palacios-Játiva P, Azurdia-Meza CA, et al. Underground mine positioning: A review. *IEEE Sens J*. 2021;22(6):4755-71.
- [6] Hancke GP, Silva BJ. Wireless positioning in underground mines: Challenges and recent advances. *IEEE Ind Electron Mag*. 2021;15(3):39-48.
- [7] Li MG, Zhu H, You SZ, et al. UWB-based localization system aided with inertial sensor for underground coal mine applications. *IEEE Sens J*. 2020;20(12):6652-69.
- [8] Adamiuk G, Zwick T, Wiesbeck W. UWB antennas for communication systems. *Proc IEEE*. 2012;100(7):2308-21.
- [9] Zhao Y, Wang M. The LOS/NLOS classification method based on deep learning for the UWB localization system in coal mines. *Appl Sci*. 2022;12(13):6484.
- [10] Höflinger F, Müller J, Zhang R, et al. A wireless micro inertial measurement unit (IMU). *IEEE Trans Instrum Meas*. 2013;62(9):2583-95.
- [11] Caron F, Duflos E, Pomorski D, et al. GPS/IMU data fusion using multisensor Kalman filtering: introduction of contextual aspects. *Inf Fusion*. 2006;7(2):221-30.
- [12] Hashim HA, Eltoukhy AEE, Vamvoudakis KG. UWB ranging and IMU data fusion: Overview and nonlinear stochastic filter for inertial navigation. *IEEE Trans Intell Transp Syst*. 2023;25(1):359-69.
- [13] Zeng Z, Liu S, Wang L. NLOS detection and mitigation for UWB/IMU fusion system based on EKF and CIR. In: 2018 IEEE 18th International Conference on Communication Technology (ICCT). IEEE; 2018. p. 376-81.
- [14] Wang L, Zhang S, Qi J, et al. Research on IMU-Assisted UWB-Based Positioning Algorithm in Underground Coal Mines. *Micromachines*. 2023;14(7):1481.
- [15] Si L, Wang Z, Wei D, et al. Fusion positioning of mobile equipment in underground coal mine based on redundant IMUs and UWB. *IEEE Trans Ind Inform*. 2023;20(4):5946-58.
- [16] Zhang J, Orlik PV, Sahinoglu Z, et al. UWB systems for wireless sensor networks. *Proc IEEE*. 2009;97(2):313-31.
- [17] Wiesbeck W, Adamiuk G, Sturm C. Basic properties and design principles of UWB antennas. *Proc IEEE*. 2009;97(2):372-85.
- [18] Cao L, Chen H, Chen Y, et al. Bio-inspired swarm intelligence optimization algorithm-aided hybrid TDOA/AOA-based localization. *Biomimetics*. 2023;8(2):186.
- [19] Elwischger BPB, Sauter T. Efficient ambiguity resolution in wireless localization systems. *IEEE Trans Ind Inform*. 2017;13(2):888-97.
- [20] Brossard M, Barrau A, Bonnabel S. AI-IMU dead-reckoning. *IEEE Trans Intell Veh*. 2020;5(4):585-95.
- [21] Feng D, Wang C, He C, et al. Kalman-filter-based integration of IMU and UWB for high-accuracy indoor positioning and navigation. *IEEE Internet Things J*. 2020;7(4):3133-46.
- [22] Bai N, Tian Y, Liu Y, et al. A high-precision and low-cost IMU-based indoor pedestrian positioning technique. *IEEE Sens J*. 2020;20(12):6716-26.

- [23] González J, Blanco JL, Galindo C, et al. Mobile robot localization based on ultra-wide-band ranging: A particle filter approach. *Robot Auton Syst.* 2009;57(5):496-507.
- [24] Poterjoy J. A localized particle filter for high-dimensional nonlinear systems. *Mon Weather Rev.* 2016;144(1):59-76.
- [25] Zhang H, Zhang J, Xue C, et al. A Sequential Sage-Husa Adaptive Filter for Cooperative Localization. In: *International Conference on Guidance, Navigation and Control*. Singapore: Springer Nature Singapore; 2024. p. 523-32.
- [26] Singh H, Mishra KV, Chattopadhyay A. Inverse unscented Kalman filter. *IEEE Trans Signal Process.* 2024.
- [27] AbdelAty AM, Yousri D, Chelloug S, et al. Fractional order adaptive hunter-prey optimizer for feature selection. *Alex Eng J.* 2023;75:531-47.